## OCCASION

This publication has been made available to the public on the occasion of the 50th anniversary of the United Nations Industrial Development Organisation.

## DISCLAIMER



## FAIR USE POLICY



## CONTACT

Please contact publications@unido.org for further information concerning UNIDO publications.

For more information about UNIDO, please visit us at www.unido.org

UNITED NATIONS INDUSTRIAL DEVELOPMENT ORGANIZATION
Vienna International Centre, P.O. Box 300, 1400 Vienna, Austria
Tel: (+43-1) 26026-0 · www.unido.org · unido@unido.org

23112

COMMISSIONER **UNIDO**

FINAL REPORT

# Assessment of the ENERMAR technology, investigating viability and efficiency of a Kobold turbine prototype

**Date:** **02 November 2005**


WRITTEN BY
Prof. Alfredo Cigada
Prof. Alberto Zasso

CONTRACT RESPONSIBILITY
Prof. Alfredo Cigada
Prof. Alberto Zasso

DEPT OF MECHANICS DIRECTOR
Prof. Giorgio Diana

**INVESTMENT AND TECHNOLOGY PROMOTION FOR MARINE CURRENT EXPLOITATION IN SOUTH EAST ASIAN COUNTRIES - PREPARATORY PHASE**

# Assessment of the ENERMAR technology, investigating viability and efficiency of a Kobold turbine prototype

Alfredo Cigada, Alberto Zasso Dipartimento di Meccanica, Politecnico di Milano

## 1. INTRODUCTION

According to Project: US/RAS/04/069, Politecnico di Milano was charged by UNIDO to start an improvement assessment process for the Kobold water turbine.
The object of the present contract is to give the aerostatic coefficients for a single vane of the same kind as those equipping the already built prototype.
Tests have been performed in Politecnico di Milano wind tunnel: results are easier to be obtained in the wind tunnel at a high reliability level and later they can be scaled to water according to well known similitude criteria. This procedure has been often performed by the research team of the wind tunnel in Politecnico di Milano, always with satisfactory results.

The final report will go through the following points:

- the wind tunnel
- the testing strategy
- the model and preliminary calculations
- the balance
- the calibration procedures
- results

## 2. POLITECNICO DI MILANO WIND TUNNEL

To the purpose of supporting by a state-of-the-art facility the world-wide recognized excellence of Politecnico di Milano research in the field of Long-Span Bridge Wind Engineering, as well as general Aerodynamics, in the late 90's it was decided to design and build a new large Wind Tunnel, having a very wide application spectrum, very high flow quality standards and a number of testing facilities. The Wind Tunnel, being a reference all over Europe for Wind Engineering applications as well as for flow-structure interaction, is working at its full capability since September 2001 and in the four years of operations it has been fully booked for applications in both fields of Wind Engineering and Aerospace applications. In addition to the already mentioned Wind Engineering projects, several Aerospace applications have been dealt with: Helicopters aerodynamics (Agusta), Air intake aerodynamics, Flying model aeroelasticity, etc.. Figure 1 shows an overview of the Wind Tunnel: it's a closed circuit facility in vertical arrangement, having two test sections, a 4x4m high speed low turbulence and a 14x4m low speed boundary layer test section. The overall wind tunnel characteristics are summarized in Table 1; the vertical arrangement and flow circuit are sketched in the vertical section of Figure 2 and Figure 3. The presence of two test sections of very different characteristics is peculiar to this facility, offering a very wide spectrum of flow conditions from very low turbulence and high speed in the contracted 4x4m section ($I_u$<0.15% - $V_{Max}$=55 m/s) to the earth boundary layer simulation in the large wind engineering test section. Focusing on the boundary layer test section, its overall size of 36m length, 14m width and 4m height allows for very large scale wind engineering simulations, as well as for setting up scale models of very large structures including wide portions of the surrounding landscape. The relevant height of the test section and its very large total area (4m, 56m$^2$) allows for very low blockage effects even if large

topographic models are included.

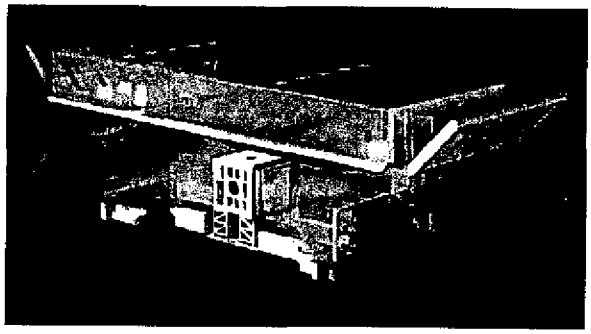

**Figure 1: Politecnico di Milano Wind Tunnel**

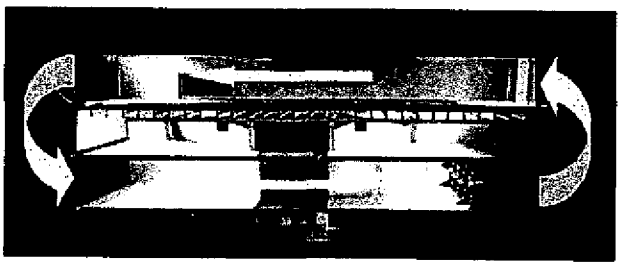

**Figure 2: Wind Tunnel section**

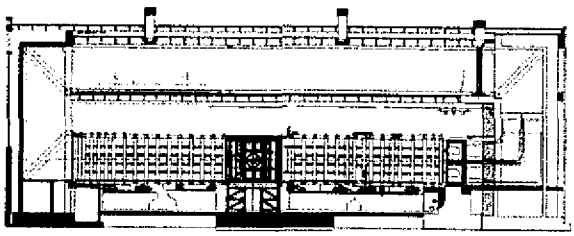

**Figure 3: Wind Tunnel section**

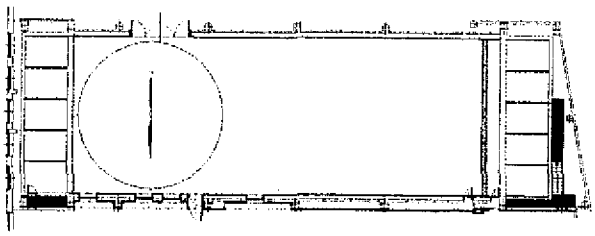

**Figure 4: Wind Tunnel top view**

The flow quality with smooth flow shows a 1.5% along wind turbulence and ±3% mean speed fluctuations in the measuring section. A very large 13m-diameter turntable lifted by air-film technology allows for fully automatic rotation of very large and heavy model fitted over it (max load 100.000 N). The device is specifically suited for very quick and easy change of wind exposure of very long span bridge aeroelastic models, avoiding all the problems related to the repetitive assembly and disassembly of those complex models (Figure 4).

The wind tunnel has a floating floor, allowing for a very clean model set-up, leaving all the instrumentation cable connections out of the flow. The very long upwind chamber is designed in order to develop a stable boundary layer and the flow conditions are very stable even when parameters like temperature are considered, due to the presence of a heat exchanger linked to the general control loop of the facility. The Wind Tunnel is operated through an array of 14 axial fans organised in two stacks of seven 2x2m independent cells. 14 independent inverters drive the fans allowing for a continuous and independent control of the rotation speed of each fan. This fully computer controlled facility can help in easily obtaining, joined to the traditional spires & roughness techniques, a very large range of wind profiles simulating very different flow conditions and very different geometrical scales. The wind tunnel process is fully controlled by a PLC and a computer network (ABB control system), monitoring through more than 100 transducers all the most important flow parameters in terms of wind speeds, pressures, temperatures, humidity, vibrations of the fans and of the structure, door opening etc., and allowing for feedback control on the flow temperature and speed.

The flow conditions were found to be very stable and a confirmation of this fact is the very low turbulence level in smooth flow. All the typical various set of spires have been developed in order to simulate the different wind profiles and an original facility has been recently installed allowing for active turbulence control in the low frequency range.

| **Politecnico di Milano Wind Tunnel** | | | | |
|---|---|---|---|---|
| **Tunnel Overall Dimensions** | | | **50×15×15 $[m]$** | |
| **Maximum Power (Fans only)** | | | **1.5 $[MW]$** | |
| **Test Section** | **Size $[m]$** | **Max Speed $[m/s]$** | **$\Delta U/U$ %** | **Turb. Int. $I_u$ %** |
| **Boundary Layer** | **14×4** | **16** | **$< \pm 3$** | **$< 1.5$** |
| **Low Turbulence** | **4×4** | **55** | **$< \pm 0.2$** | **$< 0.15$** |

**Table 1: Overall wind tunnel characteristics**

Concerning the low-turbulence high-speed section, positioned in the lower arm of the circuit, the large dimensions (4x4m) and the quite high wind speed (55 m/s) enable to reach Reynolds numbers in the order of $\mathrm{Re} = 4.5E6$. The very low levels of turbulence reached in this section (0.15%), give the facility a very wide spectrum of possible applications. A number of transducers, instrumentation and data acquisition systems are available, allowing for all the typical boundary layer wind tunnel measuring applications in the wind-engineering field.

## 3. THE TESTING STRATEGY

Prior to starting a wide range activity, a research plan has to be outlined. The leading idea is to start with the existing Kobold turbine. The overall process, which could lead to the optimal adaptation of the technology to local conditions, could be planned in different phases. These could be:

- *Assessment of the present technological development;*
- *Mathematical modelling*
- *Experimental tests on the complete turbine*
- *Optimisation*

The first phase , that is the evaluation of the existing situation, may be split into different tasks

- Setting up of a single vane model to be tested in the wind tunnel
- Setting up of a suitable load cell to measure forces
- Wind tunnel measurements
- Data analysis

This first phase deals with the experimental tests on the single vane.

The aim of the initial phase is to deal with the wind tunnel tests on a single vane. The key activities involve an in depth evaluation of the turbine wing profile in the wind tunnel, measuring both the flow field in the surrounding of a vane and the global forces given by the stream. This enables to derive the aerostatic coefficients. Of course the leading role of such a big wind tunnel is that of working with rather high scale (that is 2/3 the real profile chord in the present case), though preventing form the typical load effect problems of small test sections and related to the blockage effect.
To achieve these measurements it has been necessary to develop a dynamometric model of the turbine blade and run the necessary tests in the wind tunnel, prior to come to the final elaboration of the collected data and to the overall evaluation of the existing equipment efficiency.
In more details, the first phase has consisted in setting up a vane model, for the wind tunnel testing operation. This is an important step of the evaluation phase, as, according to the usual adopted procedures, the wind tunnel features should match those needed for the specific test to be performed.

## 4. THE MODEL AND PRELIMINARY CALCULATIONS

The vane model has been designed as light as possible in order to limit the dynamic effects on the recorded measurements and at the same time it has been built very stiff, in order to reduce any wind-structure dynamic interaction.
Therefore this operation has required particular skills in the model construction (Figure 5 and Figure 6); the model has been built using carbon fibre, with a very smooth surface painting. The adopted shape is that of the existing Kobold turbine, the so called "high lift 018".

Special care has been devoted to similitude scaling, as the real structure will operate under water, which implies very high Reynolds numbers. Testing has been performed at the highest possible Reynolds numbers (high speed, large models).

It is remembered that Reynolds number is the ratio between the fluid forces and the friction forces exerted by the fluid on the body exposed to the fluid stream. Working under similitude conditions means that this ratio is the same for the model being tested in the wind tunnel and the full-scale prototype.

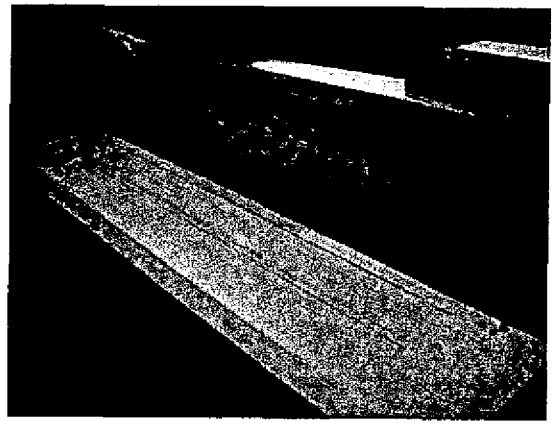

**Figure 5: building the vane model**

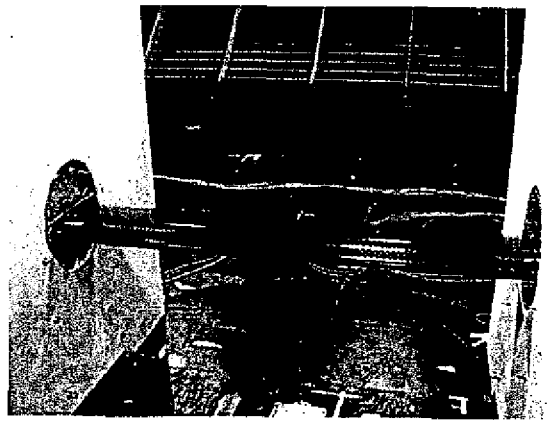

**Figure 6: the vane in the wind tunnel**

Advantage of large scale (close to full scale) wind tunnel tests is that the air cinematic viscosity is just 15 times lower than the water cinematic viscosity so that at Wind Tunnel air speed about 15 times larger than the corresponding full scale water flow Reynolds numbers very close to full scale can be achieved. This is the case of the studied Kobold turbine vane Wind Tunnel tests, where air speed much larger than the full scale water current can be applied on a close to unity scale ratio model.

With reference to the following symbols and corresponding values: $\rho$ $V$ and $\mu$ the fluid density, velocity and viscosity, $B$ the vane chord, having indicated with the suffix *"P"* and *"M"* the quantities related to Prototype and Model, with reference to the standard I.S. values $\mu_{Air} = 1.83 \cdot 10^{-5}$, $\mu_{Water} = 1.0 \cdot 10^{-3}$, $\rho_{Air} = 1.23$, $\rho_{Water} = 1.0 \cdot 10^{3}$, the ratio between prototype and scale model Reynolds Number can be represented as follows:

$$\mathrm{Re} = \frac{\rho V B}{\mu} \qquad \frac{\mathrm{Re}_P}{\mathrm{Re}_M} = \frac{\rho_{Water}}{\rho_{Air}} \frac{\mu_{Air}}{\mu_{Water}} \frac{V_{Water}}{V_{Air}} \frac{B_P}{B_M} \qquad \frac{\mathrm{Re}_P}{\mathrm{Re}_M} = 14.87 \frac{V_{Water}}{V_{Air}} \frac{B_P}{B_M}$$

Having selected a scale ratio of the model in the order of 2/3 or in other words $B_P/B_M = 3/2$, the Reynolds Number ratio prototype to model is in the order of $\mathrm{Re}_P/\mathrm{Re}_M = 22.3 \cdot V_{Water}/V_{Air}$.

Being the typical current speed in the order of $V_{Current} = 1 \div 2\, m/s$, but with a relative

speed under steady-state conditions around 2 times the current speed, then it has been assumed $V_{Water} = 2 \div 4\, m/s$, and being the tests performed at a wind speed $V_{Air} \cong 12\, m/s$ the typical Re ratio will be in the order of $Re_P/Re_M \cong 7.5$ in the worst case. In other words the wind tunnel tests will be rather closely representative of the full scale Reynolds Number. Special care will be taken to the surface roughness problem. In fact it is well known that a large roughness on the wing surface can lead to earlier flow detachment at large angles of attack and consequently to lower maximum lift allowed by the lifting surface. On the other hand a larger roughness surface is typically representative of larger Reynolds number conditions. The true vane surface, under operating conditions in the sea environment will very quickly experience a growth in its, so that it is believed that the very smooth surface tests could be representative just of laboratory conditions or brand new equipment. For these reasons both conditions were tested: smooth and rough surface Kobold turbine vane applying a very rough coating to the wing profile, (see Figure 7).

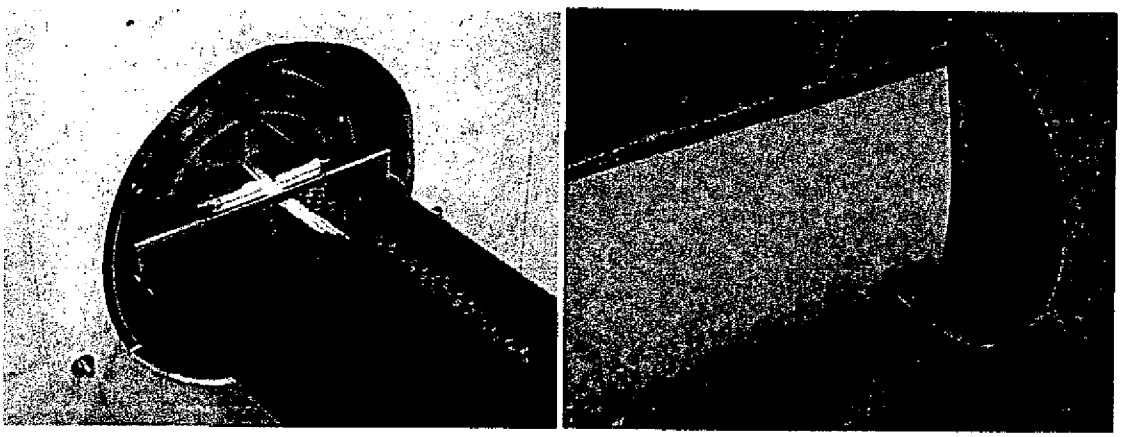

**Figure 7: the smooth and the rough wing coating**

## 5. THE BALANCE

The next step has consisted in setting up a special wind tunnel balance to get the aerostatic vane coefficients. Forces on the vane are directly measured, together with the flow speed, in order to get the aerostatic coefficients for the chosen vane profile.

Force measurement in wind tunnels is for sure a critical aspect. The overall accuracy of the measurement, is strongly influenced by different factors:

- the transducer sensitivity and full scale, according to the expected static and dynamic loads;
- the independence of the measurement from the actual load distribution along the section model, allowing for easy and effective calibration;
- load effects, if the dynamometers are not sheltered from the oncoming flow;
- "border effects", that is the reduction of the total load due to 3-D effects at the model sides;
- if dynamic measuring is asked for, both mass and stiffness have to be properly tuned to allow for a natural frequency high enough not to affect measurements; this need usually fights against the search for high sensitivity.

Two kinds of dynamometers are used to build balances for wind tunnels: those working with box models, capable of hosting the sensing elements inside of them; then those working with section models of trussed or anyway very thin structures, when it is not possible to fix any sensor inside the model, but only at the two side ends.
Details about the sensors, specially designed at Politecnico di Milano wind tunnel, are given in the following; the projects and the choices to get the best measurement performances will be analyzed, with special attention paid to those points, which may lead to too large uncertainties or to systematic effects, needing for corrections. However the dynamometer alone is not enough for getting reliable data: the supporting structure has been suitably projected to allow for rotation of the model to the desired angle of attack, though not affecting the overall performances. In the end, static and dynamic calibration will be considered. The check on border and load effects, which cannot be taken into account in laboratory calibration, but which are an essential part in the overall measurement accuracy, has also been accounted for, to complete the calibration and to assess reliable results.

The whole dynamometer set is made up of two sensors to give the global force resulting on the model under test: this force is split into the drag lift and pitch components. These components are measured in a local reference system, as the dynamometers are fixed to the model under test, and this is turned to the desired angle to change the relative wind-to-model position. To go to the "global" reference system, with components parallel and normal to the relative wind speed axes, a transformation matrix must be considered, and therefore the relative angle between the wind speed and the model reference axes must be known and measured too.

The sensors are of the strain gage kind: the choice has been led by the need of having small and easy to-handle sensors and to allow for dynamic testing at least in the range 0-10 Hz. Special attention has been paid to the strain gages thermal sheltering, to prevent form output drift. This is a critical aspect, especially due to the fact that the sensor has to be exposed to the wind flow which may cause ventilation effects. These may lead to non uniform temperature fields inside the sensor, therefore making strain gage temperature compensation useless. A sketch of the dynamometer concept is given in Figure 8.

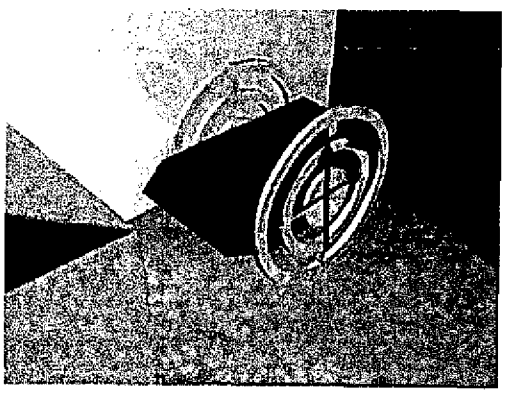

**Figure 8: external dynamometer set**

The first attempt has been for a strain gage sensor, already known in literature and made up by a number of plates (which can be considered rigid) joined by thin beams, which are the sensing elements: a force, whichever oriented in the sensor's plane, is detected

trough two normal components. However, a solution like the first in Figure 9 is not fit, as the thin beams mainly react in tension and compression: the modified final solution of Figure 9 improves sensitivity, as the load mainly causes bending strains (with strain gages it is better this latter solution also for thermal compensation). The strain gages have been glued according to the theoretical scheme of Figure 10 and Figure 11, for pitch and for each force component. In this case strain gage sheltering from the wind has been provided by suitable side screens to prevent from both load and "border" effects (non confined flow) and ventilation effects (forcing bad temperature compensation).

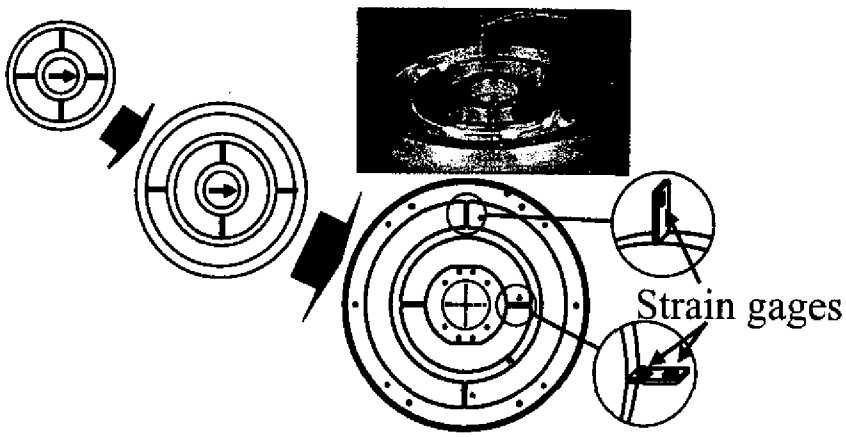


**Figure 9: external dynamometer**

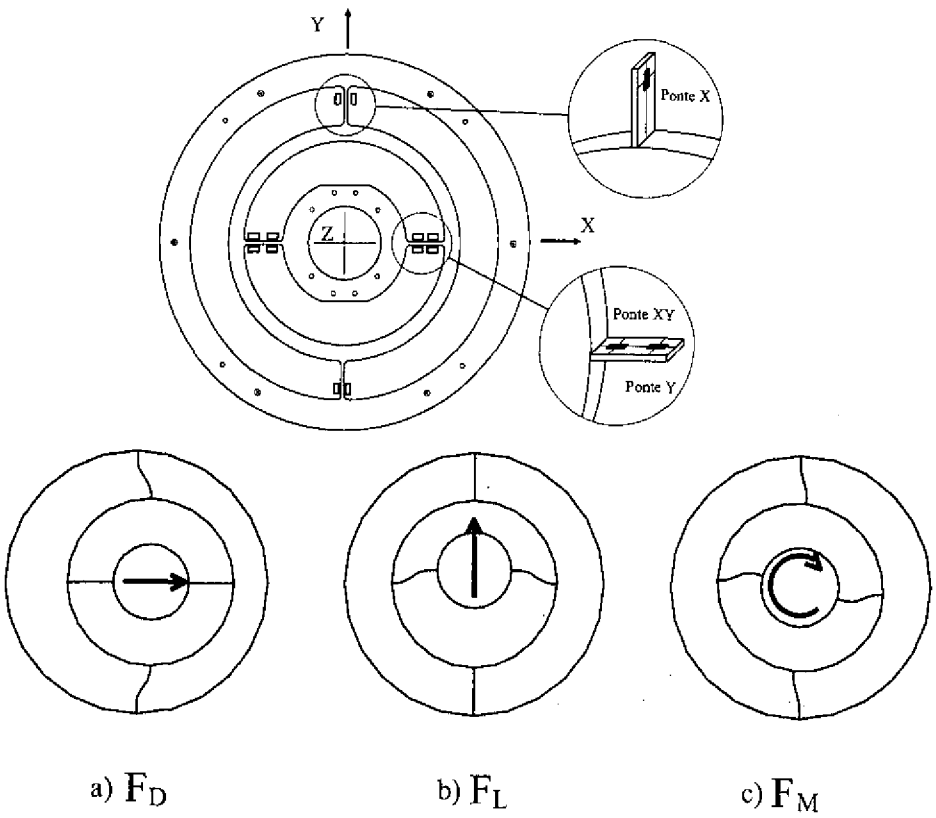


**Figure 10: details on the dynamometers**

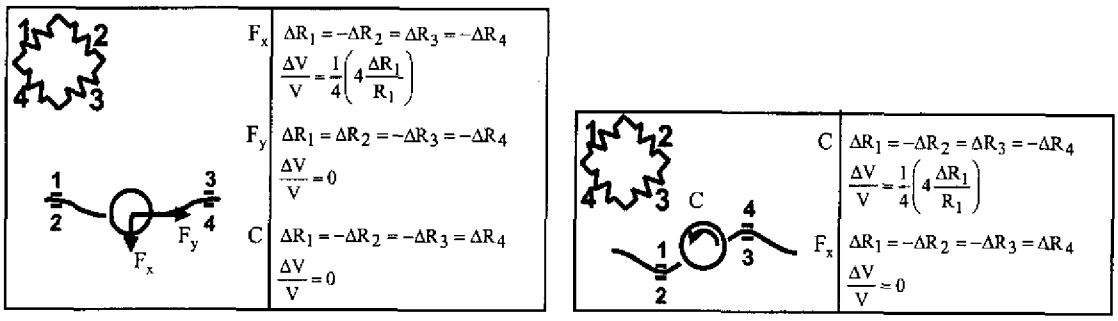


**Figure 11: external dynamometer: main idea**

For a correct dimensioning in terms of sensitivity and full scale, the dynamometers must withstand the expected loads in the wind tunnel: these have been estimated for some typical tested models. The maximum load has been estimated through considering the model weight (comprising the supporting elements), the stationary wind forces (fixed model, static coefficients), non stationary wind forces (moving model, dynamic actions) and the inertia forces; the relative weight of the 4 named forces on the overall loads have been considered: they are more or less comparable.

Some preliminary dimensioning has been performed, a prototype has been built and a F.E.M. check has been carried out on the final design before building the real dynamometer. It has therefore been possible to foresee the beams behavior due to all the possible loads, and to look for the best strain gage positions, in order to achieve a compromise in terms of linearity and sensitivity, full scale and rigidity, not forgetting dynamic measurements too.

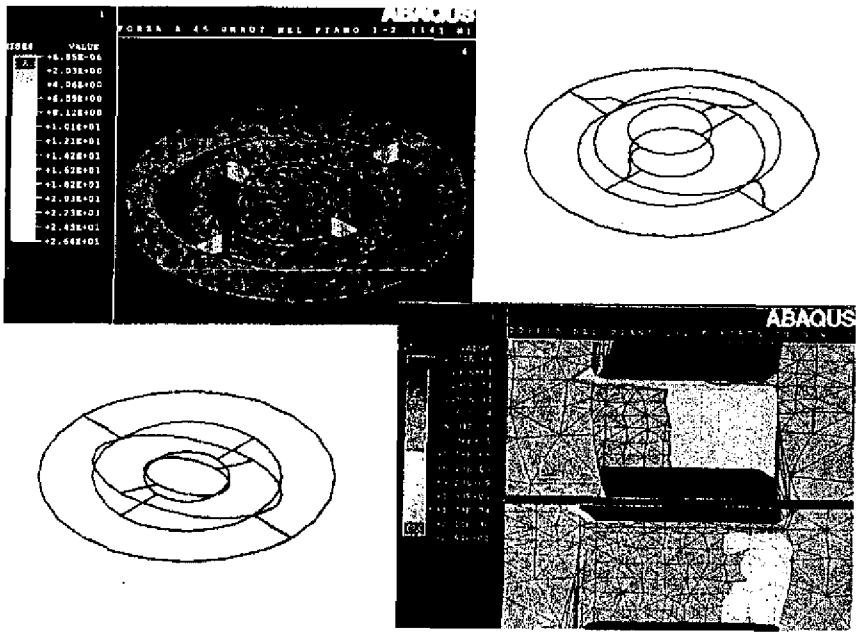


**Figure 12: the FEM model**

The mentioned preliminary dimensioning has been performed on a simple analytical model, assuming a thin beam with restrained joints at the ends and working on the theory of elasticity. The strains due to a force and a moment applied to the central plate

have been considered (see Figure 13). Concerning the two measured force components, the dynamometer exhibits the best sensitivity when strain gages are glued close to the beam ends (not too much to prevent from notch effects).

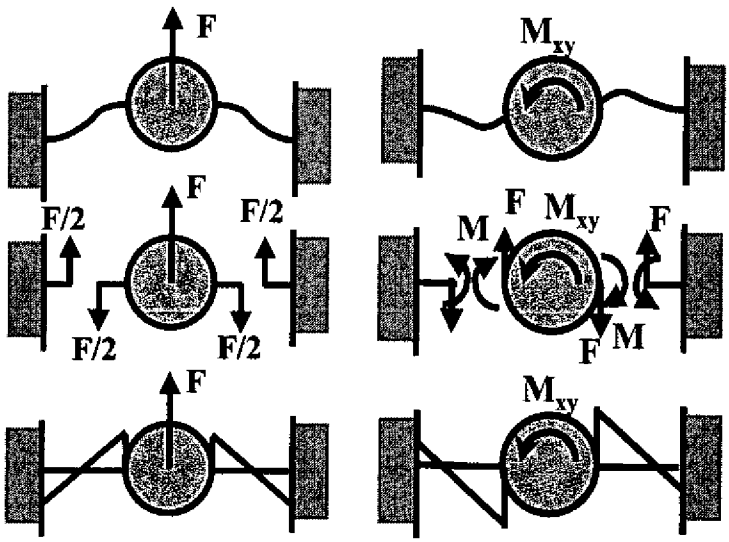


**Figure 13: internal dynamometer: dimensioning**

The sensitivity to torque is still greater for strain gages close to the extremities, but the bending moment in the thin beams is not symmetric as in the case of force, being greater at the internal side. This strain is also a function of r, that is the distance from the dynamometer center (where the moment is applied), being higher where r is lower [2]. So it comes out that the best position to glue the strain gages to sense torque is on the beams between the inner and the mid ring plates, close to the inner one. On the same beams, close to the mid ring, two other gages sense one component of the global force, while the two beams between the second and the third ring carry the strain gages to sense the other force component, normal to the previous one. A first check on a simple one component prototype has put into evidence that the estimated values for sensitivity, full scale and natural frequencies were correct within a 5% limit.

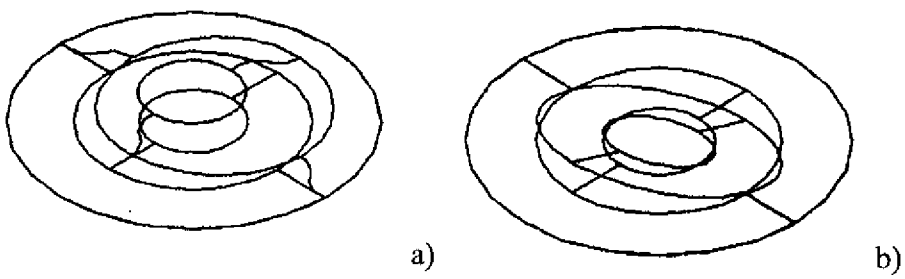


**Figure 14: a) general plane load b) out of plane load**

The final stage has been the numerical simulation via a FEM model of the whole dynamometer (by means of beam elements) and of the sensing beams alone (by means of brick elements) Figure 12 and Figure 14 show a sample of this kind of calculations. The aim was not only to have a more refined check on the dimensioning calculations, but also to foresee the sensing element behavior to different complex load conditions, such as a combination of forces with different directions superimposed to a torque. Also

loads normal to the sensing plane have been considered (Figure 14): these loads shouldn't happen, but they might. A number of tested cases have then been checked through experimentation. Table 2 shows the comparison between the results of the analytical pre-dimensioning and the FEM simulations for 3 different sensors: they are in good agreement, and this has permitted to go to the prototype for the calibration of the single sensor, hoping for good linearity under every load condition. The out-of-plane effects resulted negligible, if a good project, preventing from axial loads on the model, is arranged. Three dynamometers have been built and tested to allow a statistical analysis on their behavior; finally, the most similar two have been chosen to build the set. Some preliminary tests proved that the best performances are achieved if the whole sensor is made up of one piece only (friction and hysteresis are reduced to a minimum), though requiring a good skill when tooling the surroundings of the thin beams which could suffer of a plastic deformation. To simplify the tooling task, an aluminum alloy (Avional), has been adopted for the sensing elements. The built dynamometers have been fixed to a frame with links very similar to the real ones and the same frame was provided with devices capable of giving the desired loads for calibration.

| Sensitivity Lift [με/N] | | | |
|---|---|---|---|
| | Dyn 1 | Dyn 2 | Dyn 3 |
| Experim. | 4,37 | 3,63 | 4,73 |
| Analytical | 4,57 | 4,57 | 4,57 |
| FEM | 4,49 | 4,49 | 4,49 |

| Sensitivity Drag [με/N] | | | |
|---|---|---|---|
| | Dyn 1 | Dyn 2 | Dyn 3 |
| Experim. | 5,15 | 3,94 | 5,67 |
| Analytical | 4,57 | 4,57 | 4,57 |
| FEM | 4,56 | 4,56 | 4,56 |

| Sensitivity Pitch [με/Nm] | | | |
|---|---|---|---|
| | Dyn 1 | Dyn 2 | Dyn 3 |
| Experim. | 114,46 | 87,70 | 100,98 |
| Analytical | 98,50 | 98,50 | 98,50 |
| FEM | 102,53 | 102,53 | 102,53 |

**Table 2: Sensitivity: measured and calculated**

## 6. THE CALIBRATION PROCEDURES

### 6.1. STATIC CALIBRATION

Calibration has been performed trough certified weights: the main concerns faced at this stage were the sensitivity to the load application point and the cross sensitivity effect, that is the dynamometer response along one axis when a load is applied to the normal direction: if it had a perfect behavior it should sense 0. This is not the real case, in fact, due to small imperfections, there is always some cross sensitivity, giving no zero output where it is expected.

| Lift | Dyn 1 [με/N] | Dyn 2 [με/N] | Dyn 3 [με/N] |
|---|---|---|---|
| Sensitivity | 4,37 με/N | 3,63 με/N | 4,73 με/N |
| Linearity error | 0.09% | 0.20% | 0.09% |
| Hysteresis | 0.48% | 0.16% | 0.56% |
| Zero at unload | -0.62% | -0.62% | -0.65% |
| Strain at full scale | 128,6 με | 128,6 με | 139,2 με |
| Full scale | 29,42 N | 29,42 N | 29,42 N |

**Table 3: sensor main features: linearity error is given as the maximum distance, at a certain load, between the given measurements and the best fitting calibration line, scaled to the full scale load**

To improve reliability, a calibration matrix, instead of a simple curve, has been identified, to account for cross-sensitivity, which was the main expected problem

(Figure 15). The first calibration consisted in five cycles of load and unload from zero to 100 N, in different days, to check for sensitivity variations and also possible hysteresis. Tests have then been repeated with random loads. Calibration has been given in strain first, to check FEM calculation, and only in a second time it has been performed in force. Also a check on resolution has been done by applying a 1 kg mass and then a 1.02 kg mass, assuming this limit as the minimum resolution of interest. Table 3 shows the results obtained for the force components and the three sensors. The sensor alone shows good linearity and repeatability, with standard deviation lower than 0.05 N for force and 0.0035 N m for torque. These tests allowed a final comparison between the numerical predictions and the measured values. Table 2 shows this comparison. To justify the differences between the model and the prototype, a sensitivity analysis has been carried out on some possible error-sources, that is the strain gage position, and the uncertainty in the sensing beams thickness (neglecting notch effects at the ends). The main results were that 1 mm error in the overall positioning of the four strain gages leads to a global error of less than 4%, while 5/100 mm error in the beams thickness gives a rough 5% error. These analysis justified, at least from a qualitative point of view, the observed discrepancies. Also a check on cross sensitivity was executed, showing values lower than 0.5 % at full-scale load, corresponding to the uncertainty in the estimation of the load direction in the order of 0.5°. All the possible cross effects have been considered: the most relevant problems seem to arise when torque is considered, as this is very sensitive to even a small asymmetry in the geometry of the sensing element.

Due to these reasons, it has been stated, before applying the calibration curve, to use a calibration correction matrix; this matrix, multiplied by the measurement vector, gives the real corrected values: $\begin{bmatrix} \text{Lift}_{meas} \\ \text{Drag}_{meas} \\ \text{Pitch}_{meas} \end{bmatrix} = \begin{bmatrix} l_l & l_d & l_p \\ d_l & d_d & d_p \\ p_l & p_d & p_p \end{bmatrix} \begin{bmatrix} \text{Lift}_{applied} \\ \text{Drag}_{applied} \\ \text{Pitch}_{applied} \end{bmatrix}$, written also as

$\overline{F}_{meas} = [M]\overline{F}_{applied}\left(l_l, d_d, p_p = 1\right)$, $[M]^{-1}\overline{F}_{meas} = \overline{F}_{applied}$ , with $[M]^{-1} =$ correction matrix.

Corrections are very small, less than 1%, well below the overall target uncertainty of 5%, so that in a first approximation they can be neglected.

A final experimental check concerned drift sensitivity: a constant load applied for several hours led to variations in the order of 1%. As drift is mainly related to temperature effects, this justifies the attention paid to thermal protection of the strain gages. The effects of out plane loads, already examined by numerical FEM simulations, were checked, confirming the need of spherical low friction links between the model and the sensors, in order to minimize the undesired hyperstatic effects.

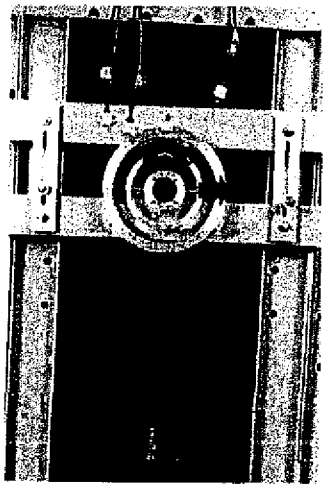

**Figure 15: calibration set-up**

### 6.2. DYNAMIC CALIBRATION

Only impulsive tests have been carried out to get the sensor natural frequencies. The experimental results confirmed the FEM predictions, showing the lowest natural frequency of interest for the sensor alone around 117 Hz. As during tests the model should be just an added mass, lowering the natural frequency, this effects has been checked for on the global frequency response function, giving 35 Hz with a 4 kg rigid model mass at each side. The final assessment is clearly dependent on the model stiffness and mass distribution.

### 6.3. ASSEMBLING

The assembling of the external dynamometer set was more critical. The two dynamometers are supported by an external frame, the section model is carried at its extremities by the inner rings of the two dynamometers (Figure 16 to Figure 18). A complete 360° rotation of the model is the functional request, together with allowance for automatic computer controlled execution of the wind tunnel tests, with high repeatability and resolution in positioning. Different solutions have been studied concerning the mechanics of the external rotating connection between the sensor and the frame. The selected scheme is shown in Figure 16 b)).

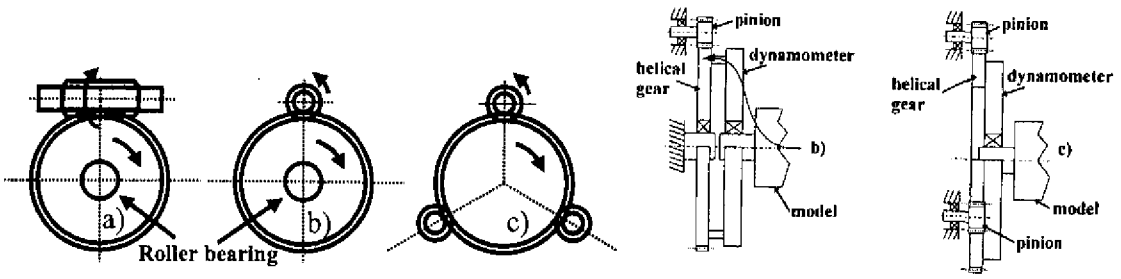


**Figure 16: different solutions for holding and moving sensors**

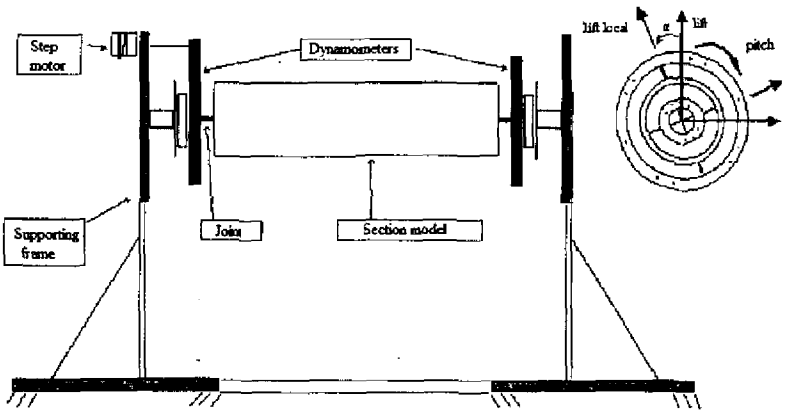


**Figure 17: the whole dynamometer assembling**

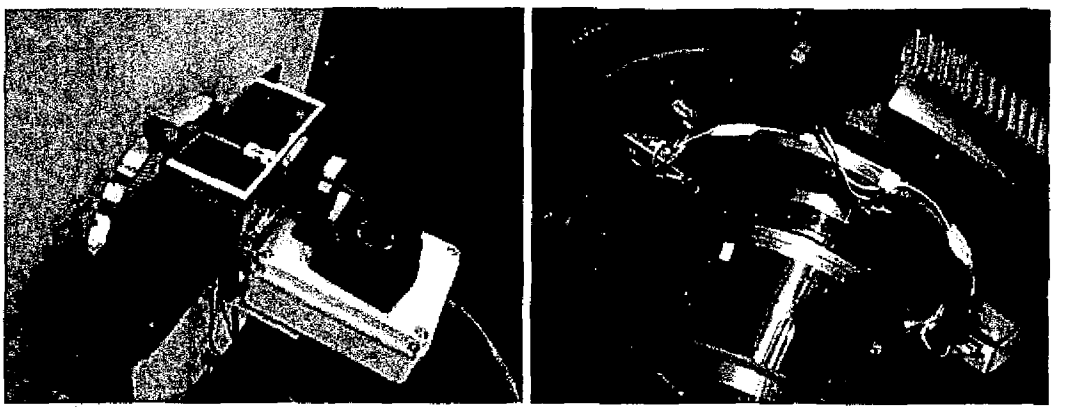

**Figure 18: details of the general assembly**

The links to the model are at the sensor inner ring, while the link to the frame is at the external ring, allowing the strain flux to pass from the first to the latter through the thin dynamometric beams, avoiding any other contact, which would affect the measurements. The external ring of one of the two sensors has been tooled and coupled to a motorized gear wheel, allowing for full 360° model rotation. The advantages of a one sided motorized sensor are obvious (no torsional hyperstatic actions, no need of controlled synchronization of the two motors). The main problems are about the request for a high model torsional stiffness to avoid deformations due to the aerodynamic loads and to the uneven torsional load on the sensors, one of them virtually free to rotate. The connections between the section model and the dynamometers play a fundamental role in the correct loading of the sensor. A special joint has been adopted (Figure 18); its equivalent cinematic behavior is the restraint of vertical, horizontal and torsional DOF, and allowance for all the other rotations and axial displacement. This virtual cinematic behavior is reached through a very low stiffness of the joint in the allowed DOF, compared with the corresponding sensor stiffness. No friction is involved, but just the stiffness of the joint metallic components, therefore producing no dissipation in case of dynamic tests. The importance of the joints is mainly due to the attempt to avoid undesired loads on the sensors, bound to model deformation, error in positioning or in other words to any hyperstatic configuration.

The dynamometric set has been finally integrated in an automatic computer-controlled procedure allowing for the measurement of the aerodynamic coefficients of a section model at different pre-defined angular positions. As far as the driving unit is concerned, a micro-stepping actuator has been selected, having torque characteristics and electronic control specially designed for compatibility with the maximum loads allowed by the sensor and suited for the dynamic characteristics of the complete dynamometric set. Inertial loads on the sensor due to the model inertia, and resonance of the motor-sensor-model chain are the main problems, leading the step motor control unit design. The angular position measurement is given directly by the open loop step-motor control, with a resolution of 0.15° corresponding to a single step. Considering that the micro-step control allows for 1/128 step resolution, it's clear that the positioning accuracy and repeatability relies essentially on the transmission mechanics. A parallel way of defining the model angular position is given by means of a MEMS accelerometer. This one, under quasi static conditions, measures the gravity acceleration component related to the device angular position according to a sine/cosine law. Figure 19 gives the results for this calibration.

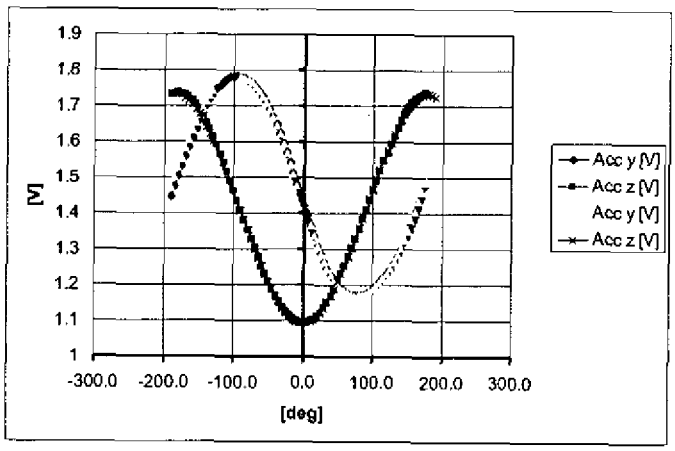


**Figure 19: accelerometer calibration**

The angular position transducer, though having a lower accuracy, compared to the nominal resolution of the open loop step-motor control, gives a redundant information, checked just in case of loss of step of the drive unit.

### 6.4. WHOLE DYNAMOMETER CALIBRATION

The calibration of the whole dynamometer, followed by the uncertainty analysis, has been repeated, as the unavoidable alignment errors of the two sensors were expected to enlarge uncertainty. Known local drag, lift and pitch loads have been provided. No sensible uncertainty enlargement has been observed. A simulation of the worst case has been performed assuming a random combination of the uncertainties playing a role in defining the drag and lift forces in a global reference system. The most significant results are the following: the single sensor maximum uncertainty is about 0.05 N with 50 N full-scale load; in global coordinates the overall uncertainty is function of the accuracy of the rotation angle measurement: with reference again to 50 N full-scale load, the global force uncertainty is 0.5 N with potentiometric angle measurement (uncertainty on rotation 0.4°), while it drops to 0.1 N with the step-motor open loop estimate (rotation uncertainty 0.1°).

## 6.5. WIND TUNNEL CALIBRATION

The wind tunnel procedure is performed in two steps: the first is aimed at checking that during transportation in the wind tunnel, no damage or any calibration change happens. Another test, seldom performed unless some problems are observed in measurements, uses tests on a NACA-0012 wing section model; this profile, having well known aerodynamic characteristics and already tested in the same wind tunnel using other kind of dynamometers, gives a good reference. This procedure is also used as a cross check, as results in terms of static coefficients need not only reliable force measurements, but also very good wind speed measurements. These are performed by means of a pitot tube and a precision micromenometer.

Figure 20, Figure 21, Figure 22 give the final calibration checks for the case of the Kobold blade.

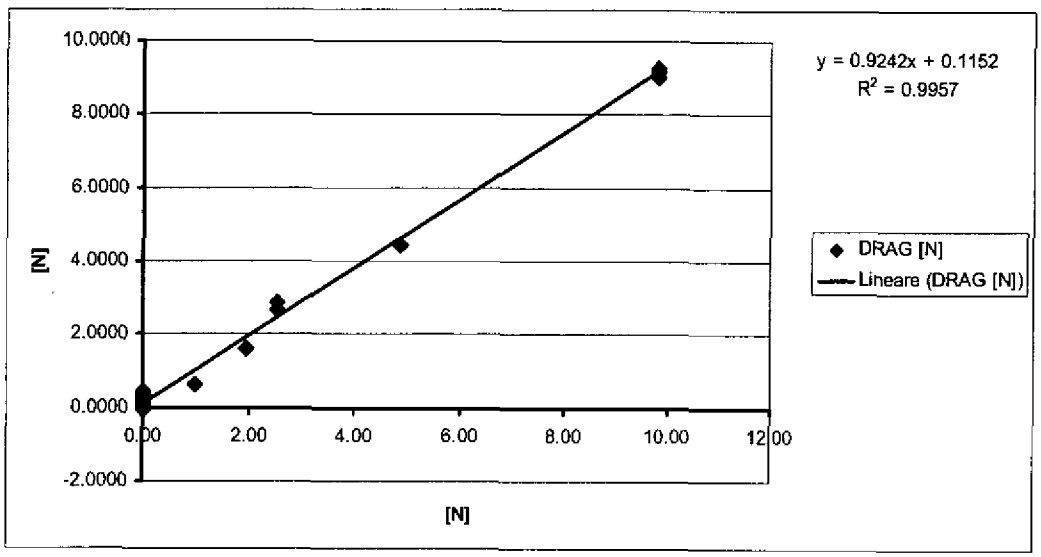


**Figure 20: final drag verification**

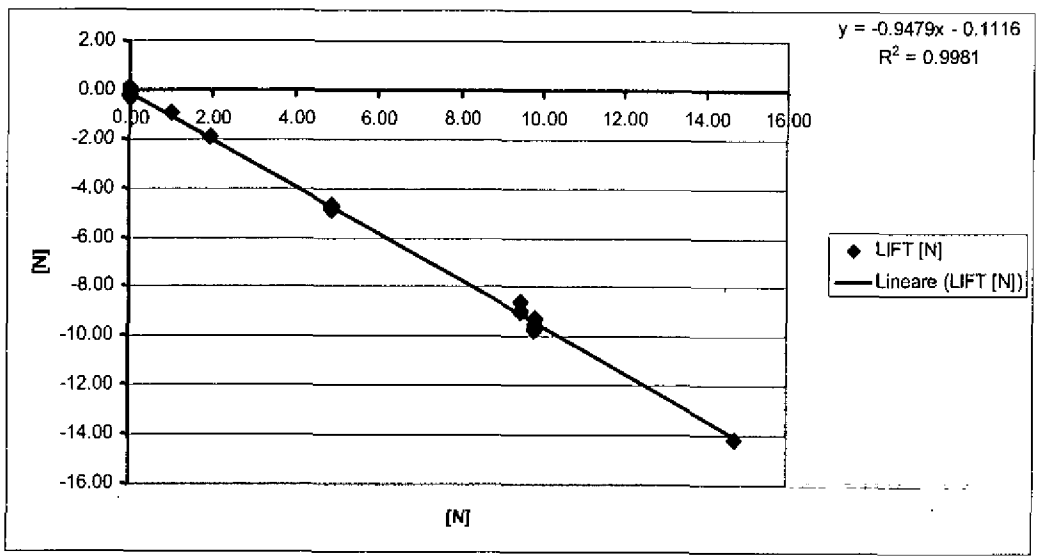


**Figure 21: final lift verification**

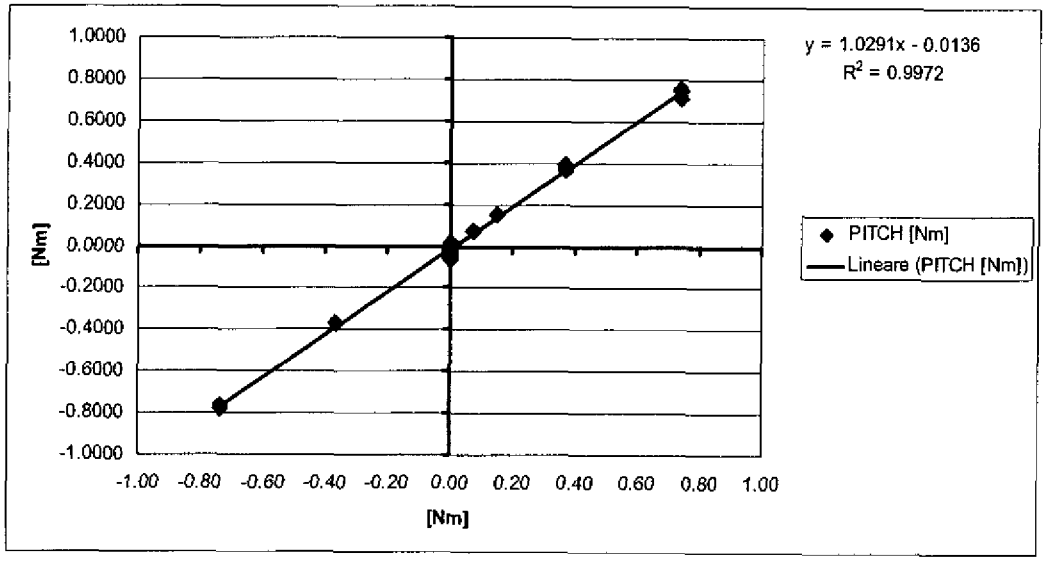


**Figure 22: final pitch verification**

## 7. RESULTS

Figure 23, Figure 24, Figure 25 show the results obtained with smooth surface. In the plots coefficients measured at different wind speeds (between 8 and 12 m/s) are shown together, as preliminary tests have proven that no difference is appreciable due to this parameter variation in the mentioned field. Measurements have been repeated, even in different days, to ensure repeatability, and very low data dispersion has been observed. Data obtained in the surrounding of +180° rotation and -180° rotation are also well superimposed each other, confirming the measurement set-up reliability.

The plots are given both in the full range -180° +180° as well as in the fundamental main working range of the wing -20° +20°. In the former, the global behaviour of the wing is studied in its full range, also including the angle of attack regions encountered just occasionally, under turbine rotation start up or strong wake conditions. In the -20° +20° range the effective wing operating conditions are studied in detail, allowing a clear understanding of its high lifting capabilities and of the corresponding low drag characteristics. As from design, quite high lift values are observed, in addition a number of points evidencing sudden flow separation/reattachment are also observed out of the operating conditions; the stall at +12° and a singular point in $C_M$ at -10° , again correlated to flow separation, are worthy being mentioned.

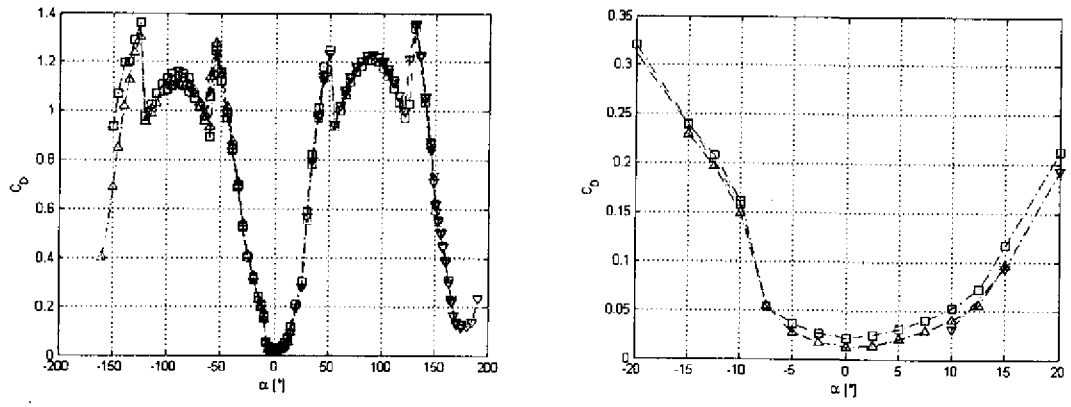


**Figure 23: $C_D$ with smooth surface: -180° +180° (left) -20° +20° (right)**

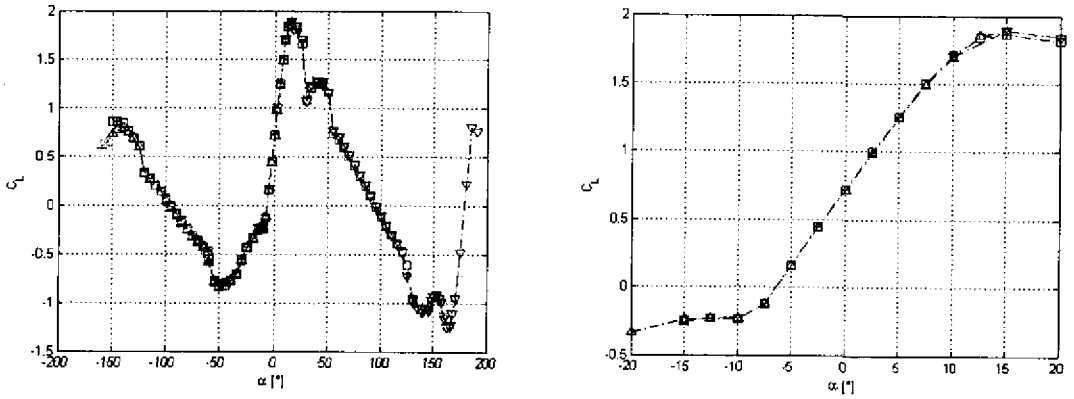


**Figure 24: $C_L$ with smooth surface: -180° +180° (left) -20° +20° (right)**

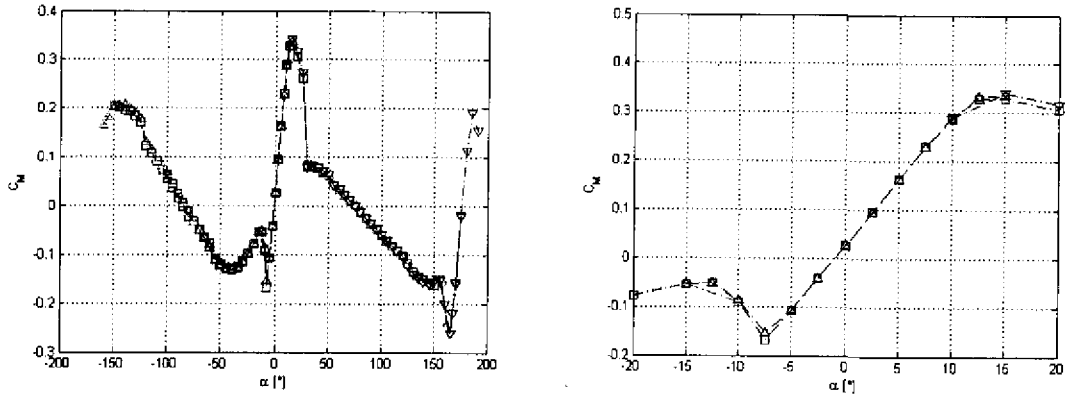


**Figure 25: $C_M$ with smooth surface: -180° +180° (left) -20° +20° (right)**

The second series of tests has been performed on the wing with increased roughness. Results are given in Figure 26, Figure 27, Figure 28 even if, for a better understanding of the roughness effects in the fundamental operating range of the wing, results from both test sessions have been then plotted together in Figure 29, Figure 30, Figure 31.

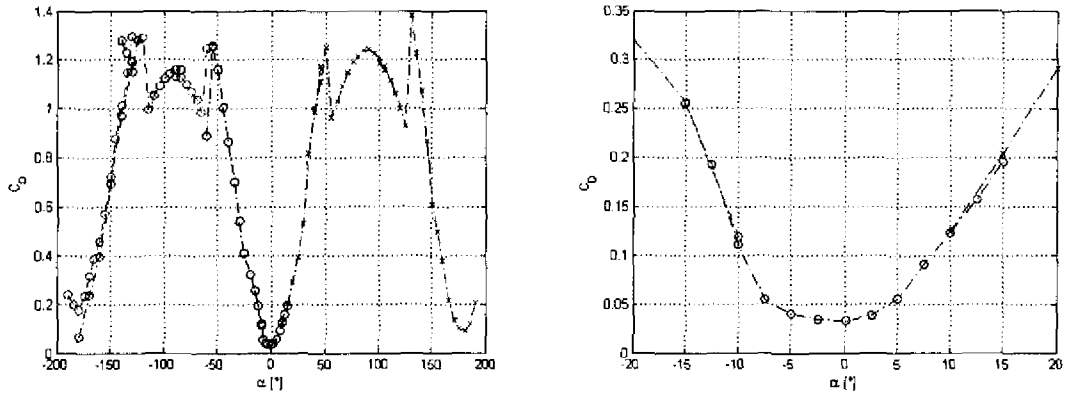


**Figure 26: $C_D$ with rough surface: -180° +180° (left) -20° +20° (right)**

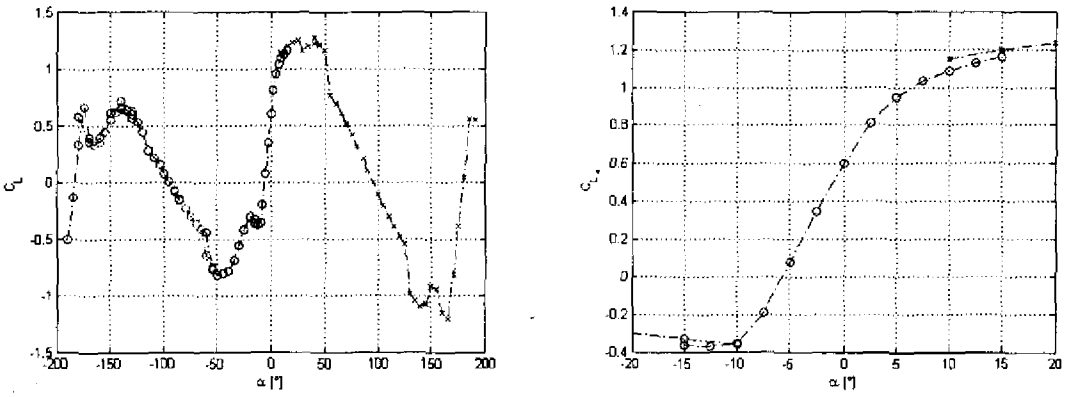


**Figure 27: $C_L$ with rough surface: -180° +180° (left) -20° +20° (right)**

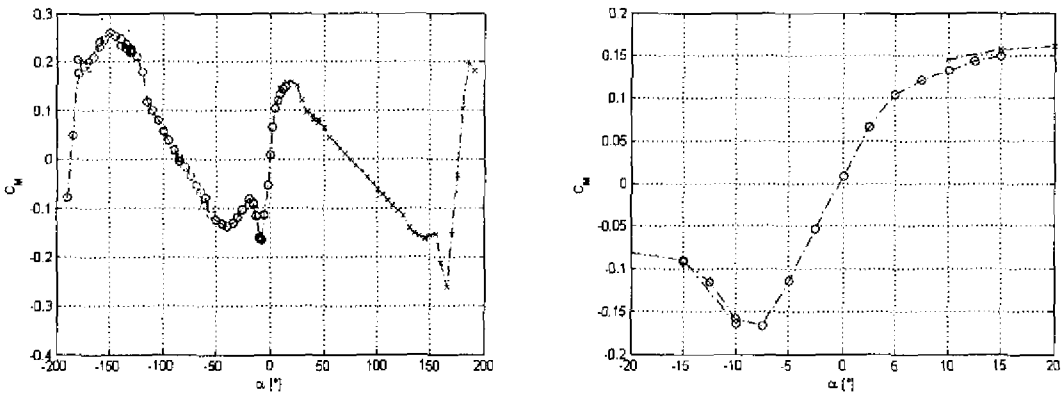


**Figure 28: $C_M$ with rough surface: -180° +180° (left) -20° +20° (right)**

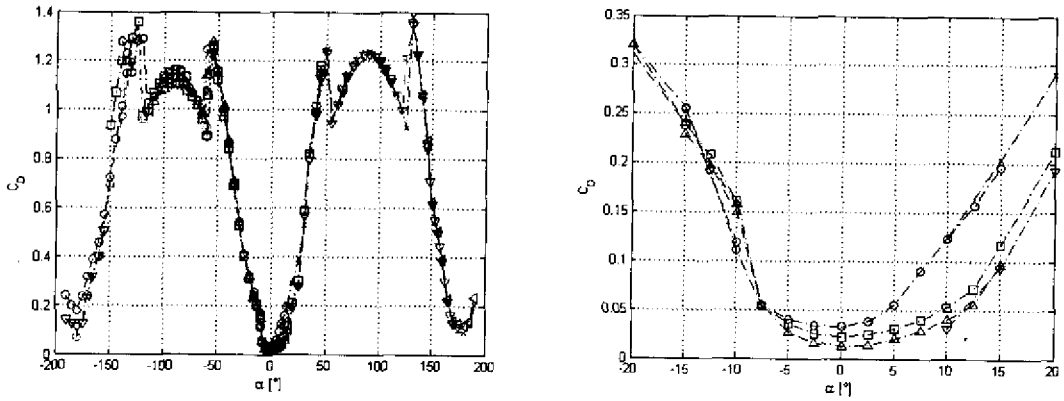


**Figure 29: $C_D$ comparison smooth and rough surface: -180° +180° (left) -20° +20° (right)**

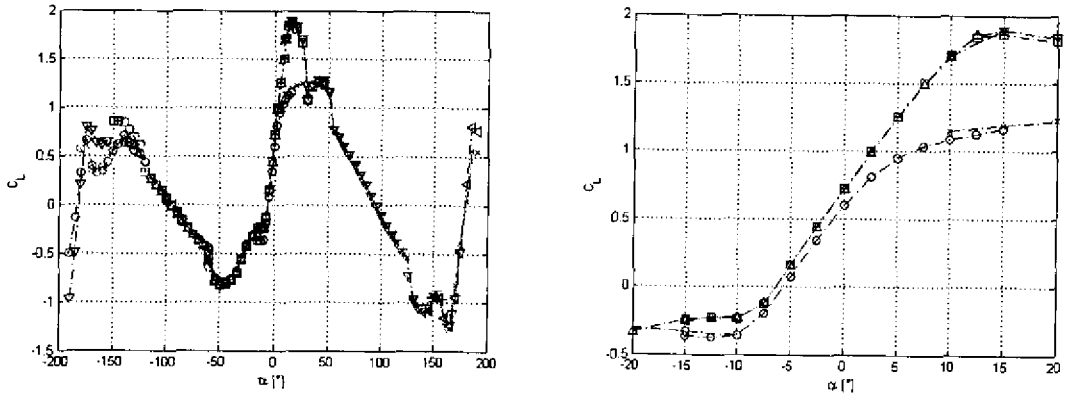


**Figure 30: $C_L$ comparison smooth and rough surface: -180° +180° (left) -20° +20° (right)**

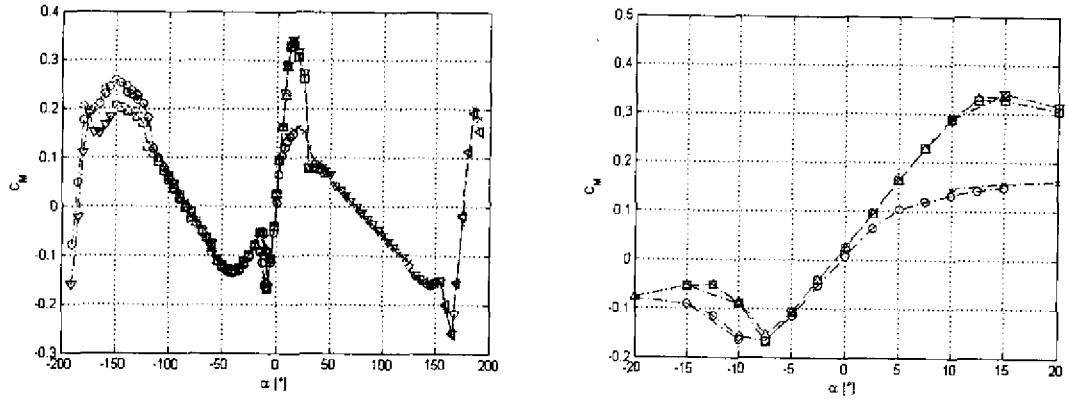


**Figure 31: $C_M$ comparison smooth and rough surface: -180° +180° (left) -20° +20° (right)**

Some facts are easily observed: as expected, due to the roughness effects, a larger drag is encountered around zero angle of attack and in the whole operating range. At the same time the large roughness anticipates separation at lower angle of attack, resulting in a quite relevant reduction of the maximum lifting capabilities of the wing. As already mentioned the Reynolds number range at which the tests were realized in the wind tunnel is somehow lower than that at full scale prototype conditions, so that it is expected that the tests are a bit conservative in the way that the full scale wing, even with the same surface roughness could show a lower reduction in the maximum lifting capabilities and a separation a bit delayed to higher angle of attack. A change is again observed when the wing offers its tail to the incoming flow, i.e. in the surrounding of -150°, when the behaviour again is that of a wing profile. For high angles of incidence, when the wing works in stalling conditions, its behaviour is typical of a bluff-body section, being much less sensitive to the different Reynolds values, and therefore exhibiting aerostatic coefficients very close each other in the two test runs.